

Spin-Triplet Superconductivity in $K_2Cr_3As_3$

Jie Yang,¹ Jun Luo,¹ Changjiang Yi,¹ Youguo Shi,¹ Yi Zhou,^{1,2} Guo-qing Zheng^{3*}

¹Institute of Physics, Chinese Academy of Sciences and
Beijing National Laboratory for Condensed Matter Physics, Beijing 100190, China

²Kavli Institute for Theoretical Sciences, CAS Center for Excellence in Topological Quantum Computation,
University of Chinese Academy of Sciences, Beijing 100190, China

³Department of Physics, Okayama University, Okayama 700-8530, Japan

*To whom correspondence should be addressed; E-mail: zheng@psun.phys.okayama-u.ac.jp

A spin-triplet superconductor can harbor Majorana bound states that can be used in topological quantum computing. Recently, $\text{K}_2\text{Cr}_3\text{As}_3$ and its variants with critical temperature T_c as high as 8 K have emerged as a new class of superconductors with ferromagnetic spin fluctuations. Here we report a discovery in $\text{K}_2\text{Cr}_3\text{As}_3$ single crystal that, the spin susceptibility measured by ^{75}As Knight shift below T_c is unchanged with the magnetic field H_0 applied in the ab plane, but vanishes toward zero temperature when H_0 is along the c axis, which unambiguously establishes this compound as a spin-triplet superconductor described by a vector order-parameter \vec{d} parallel to the c axis. Combining with points-nodal gap we show that $\text{K}_2\text{Cr}_3\text{As}_3$ is a new platform for the study of topological superconductivity and its possible technical application.

Teaser: A spin-triplet superconductor with ferromagnetic spin fluctuation superconducts at a critical temperature of 6.5 K

Introduction

In conventional superconductors, the electron pairs (Cooper pairs) are bound by the electron-phonon interaction, which results in a superconducting state with symmetric (s -wave) orbital wave function and antisymmetric spin orientation (spin singlet, $S=0$) (1). In the cuprate high temperature superconductors, Cooper pairs are also in a spin-singlet state but with d -wave symmetry for the orbital wave function, which are believed to be mediated by antiferromagnetic spin fluctuations (2). In superfluid ^3He , however, Cooper pairs are in spin triplet state ($S=1$) with p -wave orbital wave function that is antisymmetric about the origin (odd parity) (3). In this case, the spin triplet state is favored by ferromagnetic (FM) spin fluctuations. Spin-triplet

p -wave superfluid state is also believed to be realized in neutron stars (4). For long time, a solid-state analogue of ^3He has been sought in strongly correlated electron systems (SCES) where the superconducting transition temperature T_c is typically around 1 K (5–10), but unambiguous evidence is still lacking. The most promising SCES candidate had been Sr_2RuO_4 (5, 11), but recent experimental progress (12) has casted doubt on its pairing symmetry.

The spin triplet state that requires odd-parity for the orbital part of wave function is particularly fascinating and important from the topological point of view. This is because an odd-parity superconductor can be topological (13, 14) and can host Majorana bound states in their vortex cores or chiral Majorana fermions on boundary (surface or edge) (15), which are robust against scattering. Thus, spin-triplet superconductors are of great interests and importance not only in fundamental physics (16), but also in applications as their edge or bound states can be used to implement topological quantum computing based on non-Abelian statistics (17). Thus far, efforts of questing topological superconductivity have been devoted in two directions; one is via exploring bulk materials and the other is through utilizing surface states often induced by proximity effect. Physical probes aiming to identify such novel state can also be divided into two categories: bulk properties or edge states measurements. Although some progress has been made by surface-sensitive probes in looking for signatures of edge states due to superconducting proximity effect (18–21), searching for intrinsic topological superconductivity in bulk materials is highly desired. In addition to the case of odd parity, if a superconducting state breaks time reversal symmetry, the superconductivity is topological (22). Superconductivity in a crystal that breaks spatial inversion symmetry has also a good chance to be topological (23, 24).

Recently, a new superconducting family containing 3d transition-metal element Cr, $\text{A}_2\text{Cr}_3\text{As}_3$ (A = Na, K, Rb, Cs) has been reported (25–28), with a T_c as high as 8 K. Signatures for unconventional superconductivity have been found (29–34). Nuclear magnetic resonance (NMR) measurements reveal point nodes in the superconducting gap function (29, 30) and ferromag-

netic spin fluctuation in the normal state which can be tuned by changing the alkali ion radius (30). Thus, $A_2Cr_3As_3$ bear some similarities of superfluid 3He where ferromagnetic fluctuation promotes spin-triplet pairing.

The spin susceptibility in the superconducting state is a bulk property, and that measured by the Knight shift is sensitive to spin pairing symmetry. In this work, through ^{75}As Knight shift measurements in a single crystal, we show that spin nematicity (broken rotational symmetry) spontaneously emerges in the superconducting state of $K_2Cr_3As_3$ with $T_c = 6.5$ K, which is a hallmark for a spin-triplet state. We identify the direction of the vector order parameter that describes the spin-triplet state and estimate the strength of the interaction that pinned the vector to a specific crystal axis. We show that $A_2Cr_3As_3$ is a new route to studying topological superconductivity and future technical implementation using a topological spin-triplet superconductor at a high temperature.

Results

NMR spectra and determination of the Knight shift. We performed ^{75}As NMR measurements on a high-quality single crystal $K_2Cr_3As_3$ with the magnetic field H_0 applied along different directions, covering both the superconducting and normal states. Figure 1A and B show representative frequency-swept ^{75}As NMR spectra of the central transition ($I_z = -1/2 \leftrightarrow +1/2$) with $H_0 \parallel c$ axis and $H_0 \parallel ab$ plane, respectively. For axially symmetric electric field gradient (EFG), the transition frequency ν of the central transition can be written as (35)

$$\nu = (1 + K)\gamma H_0 + \frac{3\nu_Q^2}{16(1 + K)(\gamma H_0)} \sin^2\theta(1 - 9\cos^2\theta) \quad (1)$$

where K is the Knight shift, ν_Q is the nuclear quadrupole resonance (NQR) frequency, and θ is the angle between H_0 and the principal axis of the EFG at the As nucleus position. For a complete and general expression in the presence of EFG asymmetry η , see Supplementary

Materials (SM). First-principle calculation reveals that the principal EFG axis lies in the ab plane, but is along different directions for the six positions of As1 and As2 as shown in the inset of Fig. 1A (36). The obtained η is tiny ($\eta=0.004$) so that the correction to eq. (1) is negligible (see SM). In our measurements, $\theta = 90^\circ$ when $H_0 \parallel c$. For the measurements with $H_0 \parallel ab$, θ is also 90° when H_0 is parallel to the mirror planes indexed by $(2,-1,0)$, $(1,1,0)$ and $(1,-2,0)$. Such field direction can also be described by the crystal direction indices of $[1,2,0]$, $[-1,1,0]$ and $[2,1,0]$. We obtain the Knight shift K by two different methods and the results agree well. One is based on eq. (1) with the $\nu_Q(T)$ value obtained from NQR measurements (30, 31), and the other is by changing the magnetic field so that the obtained K does not depend on whether η is finite or not (see SM for details). The temperature variation of K^c for $H_0 \parallel c$ axis, and K^\perp for $H_0 \parallel ab$ ($H_0 \parallel [1,2,0]$ and equivalents) is shown in Fig. 1C and D, respectively.

Before proceeding further, we comment on some aspects of the spectra. Due to the crystal symmetry, the EFG principal axis differs by 60° between the six As positions in the plane, so the spectra with $H_0 \parallel ab$ should be 6-fold rotation symmetric when H_0 rotates in the ab plane. Indeed, we have directly confirmed this property. Figure 2 shows some representative spectra for different angle between H_0 and the a -axis of the crystal. Since As2 site has a smaller ν_Q compared to As1 (36), the central transition has two peaks and the left peak is assigned to the As2 site while the right peak to the As1 site (Fig. 1A and B). Since the As1 and As2 sites have different ν_Q values, the central transition of ^{75}As NMR spectrum with $H_0 \parallel ab$ will split into six peaks due to different θ for each As position, which was indeed observed as shown in Fig. 2A. When rotating H_0 within the ab plane, the angle dependence of the spectrum peak is 6-fold symmetric, as shown in Fig. 2C. The observed peak positions are in good agreement with those calculated from Eq. (1), with ν_Q value taken from ref. (30, 31). The two sites As1 and As2 show basically the same properties as found in previous NMR measurements (29, 31) and also in the present work (see the SM for details). We therefore focus on the As2 site hereafter.

Electron correlations. We then discuss the properties of the electron correlations based on the results of ^{75}As Knight shift and spin-lattice relaxation rate $1/T_1$. For both field orientations, the Knight shift K increases with decreasing temperature below $T = 50$ K. We also measured $1/T_1$ for the As2 site. Figure 3 shows $1/T_1T$ above T_c as a function of temperature. For each field orientation, $1/T_1T$ increases upon cooling also below $T = 50$ K. These results demonstrate that FM spin fluctuations develop at low temperatures, being consistent with the previous results obtained in polycrystalline samples (29, 30).

The absolute value of $1/T_1T$ obtained by NQR is larger than that obtained in a single crystal with $H_0 \perp c$ ($H_0 \parallel [1,2,0]$) or $H_0 \parallel c$. This is because in the NQR measurements, the effective H_0 direction is along the principal axis, which is perpendicular to both the c -axis and the $[1,2,0]$ direction. As the hyperfine coupling is anisotropic in general, the absolute value of $1/T_1T$ along different direction can be different. As we show below, however, the temperature dependence of $1/T_1T$ for all field directions is identical. In general, $1/T_1T$ is proportional to the q -summed imaginary part of transverse dynamical susceptibility χ''_{\perp} divided by ω ,

$$\frac{1}{T_1T} \propto \sum_q A(q)^2 \frac{\chi''_{\perp}(q, \omega)}{\omega} \quad (2)$$

where $\mathbf{A}(\mathbf{q})$ is the hyperfine coupling tensor and ω is Larmor frequency. When there is a peak in a specific $q = Q$ due to electron correlations, $1/T_1T$ may be decomposed into two parts,

$$1/T_1T = (1/T_1T)_{\text{DOS}} + (1/T_1T)_Q \quad (3)$$

The first term is due to non-correlated electrons, being determined by the density of states (DOS) at the Fermi level, which is usually constant. The second term is due to the development of ferromagnetic spin fluctuation in the present case ($Q=0$). According to Moriya's theory for a ferromagnetically correlated 3D metal (37), $1/T_1T$ follows a Curie-Weiss T -dependence as

$$(1/T_1T)_Q = b/(T + \theta) \quad (4)$$

Figure 3 shows the fittings of $1/T_1T$ to Eq. (3), which reveals that the single-crystal data can be fitted by using $(1/T_1T)_{\text{DOS}}^c = (1/T_1T)_{\text{DOS}}^{\perp c} (H_0 \parallel [1,2,0]) = 0.18 \text{ sec}^{-1}\text{K}^{-1}$, and with the same $\theta \sim 10 \text{ K}$ obtained from the NQR data (30).

Separating various contributions to the Knight shift. Next we discuss the various contributions to the Knight shift in the superconducting state. The Knight shift K consists of three parts, $K = K_s + K_{\text{orb}} + K_{\text{dia}}$, where K_s is proportional to the spin susceptibility χ_s , K_{orb} is the contribution from orbital susceptibility and is temperature independent, and K_{dia} arises from diamagnetism due to vortex lattice formation in the superconducting state. The K_{dia} is calculated to be negligible in $\text{K}_2\text{Cr}_3\text{As}_3$ because of a large penetration depth (see SM). The K_{orb} was determined by an analysis utilizing the relationship between K and $1/T_1T$, and its value is respectively indicated by the horizontal arrow in Fig. 1C and D.

In the following we elaborate how the K_s and K_{orb} are separated. We first note that K_s can further be decomposed into two parts, with the first part K_{DOS} due to non-interacting electrons, and the second part due to d -electrons, K_s^{int} , which is T -dependent. As described above, the interacting d -electrons are responsible for FM fluctuation and contribute to the Curie-Weiss behaviour of $1/T_1T$ which is proportional to $\chi(\mathbf{q} = 0)$. In such FM spin fluctuation case, K_s^{int} is also proportional to $\chi(\mathbf{q} = 0)$ (37). Figure 4 shows the K vs. $1/T_1T$ plots with $H_0 \parallel c$ for $T_c(H) = 5.1 \text{ K} \leq T \leq 200 \text{ K}$, and with $H_0 \perp c$ ($H_0 \parallel [1,2,0]$) for $T_c(H) = 4.9 \text{ K} \leq T \leq 25 \text{ K}$, respectively. In both cases, a fairly good linear relation is indeed found, reflecting the relationship described above. The vertical dashed line indicates the position of $(1/T_1T)_{\text{DOS}} = 0.18 \text{ sec}^{-1}\text{K}^{-1}$ obtained from Fig. 3 (see preceding subsection). The corresponding K indicated by the horizontal dotted line is then $K_{\text{DOS}} + K_{\text{orb}}$. Below, we separate K_{DOS} and K_{orb} .

$(1/T_1T)_{\text{DOS}}$ and K_{DOS} should obey the Korringa relation,

$$\frac{1}{(T_1T)_{\text{DOS}}} = \frac{1}{S} \frac{4\pi k_B}{\hbar} \left(\frac{\gamma_n}{\gamma_e}\right)^2 K_{\text{DOS}}^2 \quad (5)$$

where $\gamma_{n,e}$ is the nuclear (electron) gyromagnetic ratio, and $S = 1$ in the original Korringa theory (38). From this we obtained $K_{\text{DOS}} = 0.12\%$. There exist many sources that make S deviate from 1 (39), including an anisotropy of g -factor which is expected to be small for Cr-based compounds though. Therefore, we estimate the uncertainty for K_{DOS} by allowing a 20% uncertainty for S . If we adopt $S = 1.2$ or 0.8 to estimate the errors, the upper and lower bound for K_{DOS}^c are 0.14% and 0.11% , respectively. We thus obtain $K_{\text{orb}}^c = 0.27\%(+0.01\%/-0.02\%)$. By the same manner, $K_{\text{orb}}^{\perp c} = 0.09\%(+0.01\%/-0.02\%)$ is obtained.

Spin susceptibility in the superconducting state. Now we present the main findings of this work, namely, the spin susceptibility in the superconducting state. Detailed measurements reveal that $K_s^{\perp c}$ for $H_0 \parallel ab$ and K_s^c for $H_0 \parallel c$ axis show very different behavior in the superconducting state, in contrast to $1/T_1$ which drops clearly below T_c for both field directions (Fig. S5). As shown in Fig. 5, $K_s^{\perp c}$ does not decrease upon cooling through the superconducting transition down to the lowest temperature measured, while K_s^c is reduced significantly at low temperatures and vanishes toward $T = 0$. To appreciate more visibly the anisotropic variation of K , we show in Figure 6A and B typical spectra in the superconducting state for H_0 along the c axis and in the ab plane along the $[1,2,0]$ (mirror-plane) direction, respectively. There, it can be seen that, the spectrum remains almost unchanged below $T_c = 4.9$ K for $H_0 \parallel ab$, but clearly shifts to a lower frequency below $T_c = 5.1$ K for $H_0 \parallel c$ axis. Notice that, for a spin-singlet superconductor, the spin susceptibility decreases in all directions and vanishes at zero temperature, and that even an inclusion of a strong spin-orbit coupling cannot account for the anisotropic reduction of the Knight shift (24). Also, the invariant Knight shift for $H_0 \parallel ab$ cannot be attributed to a pair-breaking effect due to a magnetic field as the upper critical field is even larger for this field configuration. However, Cooper pairs with spin-triplet pairing have internal degrees of freedom and the spin susceptibility below T_c can stay unchanged for some directions but is reduced along a certain direction.

Discussion

The $\vec{d}(\vec{k})$ vector is widely adopted to describe the order parameter of a spin-triplet superconducting state (5, 40), which is perpendicular to the spins that comprise a Cooper pair and behaves like a rotation vector in spin space. For $H_0 \parallel \vec{d}(\vec{k})$, K_s is reduced below T_c , while it is unchanged for $H_0 \perp \vec{d}(\vec{k})$. In superfluid ^3He , there is no crystal lattice, hence $\vec{d}(\vec{k})$ vector can rotate freely so that spin rotation symmetry is preserved (3). In solid spin-triplet superconductors, $\vec{d}(\vec{k})$ vector is usually along a certain crystal axis so that spin rotation symmetry is spontaneously broken (spin nematicity emerges spontaneously). In the presence of crystal disorder and spin-orbit coupling, $\vec{d}(\vec{k})$ vector can further be pinned to a particular direction among multiple equivalent crystal axes (14).

Therefore, our results indicate that Cooper pairs in $\text{K}_2\text{Cr}_3\text{As}_3$ are in a spin-triplet state, with the $\vec{d}(\vec{k})$ vector along the c axis. Such spin-triplet state possesses internal degrees of freedom and will provide a good opportunity to explore novel phenomena such as collective modes of the order parameter, half-quantum vortices, etc. An exotic feature seen from Fig. 5B is that K_s^c starts to drop at a temperature T^* that is lower than T_c . It is emphasized that both the NMR intensity and $1/T_1$ drop sharply at T_c (Fig. S4, S5). In particular, the former quantity is measured under exactly the same condition as K , which assure that the measured T_c represents the intrinsic superconducting transition temperature. The temperature difference between T^* and T_c increases with increasing magnetic field, and K_s^c even shows no reduction for $H_0 = 16$ T although this field is smaller than H_{c2} . Figure 7 shows T^* and $T_c(H)$ obtained under different fields. There is no evidence showing another phase transition in this temperature range from the electromagnetic, heat transport measurements or our NMR spectra. Therefore, the $H - T$ phase diagram of Fig. 7 is ascribed to a unlocking of the $\vec{d}(\vec{k})$ vector by the magnetic field. The curve shown by the broken lines represents the pinning force in terms of field (pinning field

) H^* above which Zeeman energy wins so that the $\vec{d}(\vec{k})$ vector originally pinned to the c -axis direction is unlocked and rotates 90 degrees. Recall that the $\vec{d}(\vec{k})$ vector is perpendicular to the Cooper-pair spins. H^* is no larger than 13 T. Also note that such $\vec{d}(\vec{k})$ vector depinning to gain Zeeman energy is different from the $\vec{d}(\vec{k})$ -vector rotation between two nearly-degenerate states (41).

In passing, we make two comments. First, a tiny change of the Knight shift was found below T_c along specific crystal directions of a strongly-correlated material UPt_3 (42), but the interpretation of the result is controversial (6), as the change is less than 1% of the total Knight shift. Second, inversion symmetry is broken in $\text{K}_2\text{Cr}_3\text{As}_3$ so that parity mixing can occur. However, the band splitting due to inversion-symmetry breaking is about 60 meV (43), which is comparable to all spin-singlet noncentrosymmetric superconductors including $\text{Li}_2\text{Pd}_3\text{B}$ (44). Therefore, parity mixing should be small in the present case. In fact, if a parity mixing takes place, it is the singlet component that is mixed. Then, one should see a certain decrease in the Knight shift even for $H \parallel ab$. However, we do not observe such behavior.

Finally, we discuss the orbital wave function of the Cooper pairs in $\text{K}_2\text{Cr}_3\text{As}_3$. Density function theory calculations show that there are three bands across the Fermi level, namely, two quasi one-dimensional (1D) bands α and β , and one three-dimensional (3D) band γ (43). The γ band makes the dominant contribution (75%) to the density of states. Previous spin-relaxation rate study has revealed point nodes in the gap function (29, 30). For a 3D Fermi surface, group theory analysis shows that in the spin-triplet pairing channel, gap functions with both point nodes and line nodes are allowed (see SM). In the case of point nodal gap, all the point nodes are located at the two poles on the Fermi surface with $k_x = k_y = 0$, as listed in Table I. Among them, only E' states ($p_x + ip_y$ and $p_x - ip_y$) are consistent with our Knight shift result with the quantum axis along the c axis direction. Notice that, for all possible E' states which are linear combinations of two basis functions, the two states listed in Table I are energetically favored,

since the $\vec{d}(\vec{k})$ -vector is along the \vec{z} direction. (45, 46). Such a state breaks time reversal symmetry and is consistent with zero-field μ SR measurement that revealed evidence for a spontaneous appearance of a weak internal magnetic field below T_c (34).

An E' state is analogous to the A phase (or Anderson-Brinkman-Morel state) in superfluid ^3He (3), and was initially proposed as a superconducting state for Sr_2RuO_4 (11) but not supported by the recent experiment (12). Such state is topological, therefore Majorana zero modes can be expected in vortex cores (47, 48). In particular, if a superconducting thin film of $\text{K}_2\text{Cr}_3\text{As}_3$, with its thickness smaller than the superconducting coherence length, is available, a single Majorana zero mode will be expected in the core of a half-quantum vortex. Thus, our results demonstrate that $\text{K}_2\text{Cr}_3\text{As}_3$ is a new platform for basic research of topological materials and possible technical applications of topological superconductivity. We also hope that our work will stimulate more precise measurements using single crystals to look for novel phenomena arising from the internal degrees of freedom of spin triplet pairing, including multiple phases and those aforementioned.

Materials and methods

Sample preparation

High quality single crystal $\text{K}_2\text{Cr}_3\text{As}_3$ samples used in this work were grown by self-flux method as described in Ref. (25). First, the starting materials KAs and CrAs were prepared by reacting K pieces, Cr powder and As powder. The mixture of KAs and CrAs with a molar ratio of 6:1 was placed in an alumina crucible and sealed in evacuated Ta crucible and quartz tube. They were then sintered at 1273 K for 24 h, followed by cooling down at 1 K/h. Extra flux was removed to obtain single crystals by centrifugation at 923 K. The single crystals are straight, thin and needle-like, with typical length of 5 mm and diameter of tens of microns. The c axis of the crystal is easy to recognize, which is along the direction of the needle. The sample

quality was checked by dc susceptibility, which shows $T_c \approx 6.5$ K at zero field. During the NMR experiments, T_c was confirmed by measuring the inductance of the NMR coil. The sharp decrease of $1/T_1$ below T_c further ensures the high sample quality.

NMR measurements

For NMR measurements with the magnetic field parallel to the ab plane, only one needle was used. For NMR measurements along the c axis, several needles were selected and aligned together. Because the $\text{K}_2\text{Cr}_3\text{As}_3$ sample is fragile and air-sensitive, the sample handling was done in an Ar-protected glove box. The ^{75}As (nuclear spin $I = 3/2$ with nuclear gyromagnetic ratio $\gamma = 7.2919$ MHz/T) NMR measurements were carried out by using a phase-coherent spectrometer. The NMR spectra were obtained by scanning the frequency point by point and integrating the spin echo at a fixed magnetic field H_0 . The spin echo was observed by using a standard $\pi/2 - \tau - \pi$ pulse sequence with $\pi/2$ pulse length of $7 \mu\text{s}$ and $\tau = 40 \mu\text{s}$. An Attocube piezo horizontal rotator was used for angle-variated NMR measurements of $H_0 \parallel ab$ plane. The angle repeatability is 50 m° and the resolution is 6 m° for the rotator. Two orthogonal Hall bars were placed on the sample holder to check the field orientation and to ensure the rotation axis being perpendicular to the applied magnetic field. The spin-lattice relaxation rate $1/T_1$ was measured by the saturation-recovery method, and determined by a good fitting of the nuclear magnetization to $1 - M(t)/M(\infty) = 0.1\exp(-t/T_1) + 0.9\exp(-6t/T_1)$, where $M(\infty)$ and $M(t)$ are the nuclear magnetization in the thermal equilibrium and at a time t after the saturating pulse, respectively.

References and Notes

1. J. L. Bardeen, N. Cooper, J. R. Schrieffer, Theory of Superconductivity. *Phys. Rev.* **108**, 1175 (1957).

2. C. C. Tsuei, J. R. Kirtley, Pairing symmetry in cuprate superconductors. *Rev. Mod. Phys.* **72**, 969 (2000).
3. A. J. Leggett, A theoretical description of the new phases of liquid ^3He . *Rev. Mod. Phys.* **47**, 331 (1975).
4. D. Page, M. Prakash, J. M. Lattimer, A. W. Steiner, Rapid Cooling of the Neutron Star in Cassiopeia A Triggered by Neutron Superfluidity in Dense Matter. *Phys. Rev. Lett.* **106**, 081101 (2011).
5. Y. Maeno, H. Hashimoto, K. Yoshida, S. Nishizaki, T. Fujita, J. G. Bednorz, F. Lichtenberg, Superconductivity in a layered perovskite without copper. *Nature* **372**, 532 (1994).
6. R. Joynt, L. Taillefer, The superconducting phases of UPt_3 . *Rev. Mod. Phys.* **74**, 235 (2002).
7. S. S. Saxena, P. Agarwal, K. Ahilan, F. M. Grosche, R. K. W. Haselwimmer, M. J. Steiner, E. Pugh, I. R. Walker, S. R. Julian, P. Monthoux, G. G. Lonzarich, A. Huxley, I. Sheikin, D. Braithwaite, J. Flouquet, Superconductivity on the border of itinerant-electron ferromagnetism in UGe_2 . *Nature* **406**, 587 (2000).
8. D. Aoki, A. Huxley, E. Ressouche, D. Braithwaite, J. Flouquet, J.-P. Brison, E. Lhotel, C. Paulsen, Coexistence of superconductivity and ferromagnetism in URhGe . *Nature* **416**, 613 (2001).
9. N. T. Huy, A. Gasparini, D. E. de Nijs, Y. Huang, J. C. P. Klaasse, T. Gortenmulder, A. de Visser, A. Hamann, T. Gorlach, H. von Lohneysen, Superconductivity on the Border of Weak Itinerant Ferromagnetism in UCoGe . *Phys. Rev. Lett.* **99**, 067006 (2007).

10. S. Ran, C. Eckberg, Q-P. Ding, Y. Furukawa, T. Metz, S. R. Saha, I-L. Liu, M. Zic, H. Kim, J. Paglione, N. P. Butch, Nearly ferromagnetic spin-triplet superconductivity. *Science* **365**, 684 (2019).
11. T. M. Rice, M. Sigrist, Sr₂RuO₄: an electronic analogue of ³He? *J. Phys. Condens. Matter* **7**, L643 (1995).
12. A. Pustogow, Yongkang Luo, A. Chronister, Y.-S. Su, D. A. Sokolov, F. Jerzembeck, A. P. Mackenzie, C. W. Hicks, N. Kikugawa, S. Raghu, E. D. Bauer, S. E. Brown, Constraints on the superconducting order parameter in Sr₂RuO₄ from oxygen-17 nuclear magnetic resonance. *Nature* **574**, 72 (2019).
13. L. Fu, E. Berg, Odd-Parity Topological Superconductors: Theory and Application to Cu_xBi₂Se₃. *Phys. Rev. Lett.* **105**, 097001 (2010).
14. K. Matano, M. Kriener, K. Segawa, Y. Ando, Guo-qing Zheng, Spin-rotation symmetry breaking in the superconducting state of Cu_xBi₂Se₃. *Nat. Phys.* **12**, 852 (2016).
15. F. Wilczek, Majorana returns. *Nat. Phys.* **5**, 614 (2009).
16. X. L. Qi, S. C. Zhang, Topological insulators and superconductors. *Rev. Mod. Phys.* **83**, 1057 (2011).
17. A. Y. Kitaev, Unpaired Majorana fermions in quantum wires. *Physics-Uspekhi* **44**, 131 (2001).
18. L. Fu, C. L. Kane, Superconducting proximity effect and Majorana fermions at the surface of a topological insulator. *Phys. Rev. Lett.* **100**, 096407 (2008).

19. V. Mourik, K. Zuo, S. M. Frolov, S. R. Plissard, E. P. A. M. Bakkers, L. P. Kouwenhoven, Signatures of Majorana fermions in hybrid superconductor-semiconductor nanowire devices. *Science* **336**, 1003 (2012).
20. H. H. Sun, K. W. Zhang, L. H. Hu, C. Li, G. Y. Wang, H. Y. Ma, Z. A. Xu, C. L. Gao, D. D. Guan, Y. Y. Li, C. H. Liu, D. Qian, Y. Zhou, L. Fu, S. C. Li, F. C. Zhang, J. F. Jia, Majorana Zero Mode Detected with Spin Selective Andreev Reflection in the Vortex of a Topological Superconductor. *Phys. Rev. Lett.* **116**, 257003 (2016).
21. D. Wang, L. Kong, P. Fan, H. Chen, S. Zhu, W. Liu, L. Cao, Y. Sun, S. Du, J. Schneeloch, R. Zhong, G. Gu, L. Fu, H. Ding, H.-J. Gao, *Science* **362**, 333 (2018).
22. T. Senthil, J. B. Marston, M. P. A. Fisher, Spin quantum Hall effect in unconventional superconductors. *Phys. Rev. B* **60**, 4245-4254 (1999).
23. M. Sato, S. Fujimoto, Topological phases of noncentrosymmetric superconductors: Edge states, Majorana fermions, and non-Abelian statistics. *Phys. Rev. B* **79**, 094504 (2009).
24. M. Nishiyama, Y. Inada, G.-q. Zheng, Spin Triplet Superconducting State due to Broken Inversion Symmetry in $\text{Li}_2\text{Pt}_3\text{B}$. *Phys. Rev. Lett.* **98**, 047002 (2007).
25. J. K. Bao, J. Y. Liu, C. W. Ma, Z. H. Meng, Z. T. Tang, Y. L. Sun, H. F. Zhai, H. Jiang, H. Bai, C. M. Feng, Z. A. Xu, G. H. Cao, Superconductivity in Quasi-One-Dimensional $\text{K}_2\text{Cr}_3\text{As}_3$ with Significant Electron Correlations. *Phys. Rev. X* **5**, 011013 (2015).
26. Z. T. Tang, J. K. Bao, Y. Liu, Y. L. Sun, A. Ablimit, H. F. Zhai, H. Jiang, C. M. Feng, Z. A. Xu, G. H. Cao, Unconventional superconductivity in quasi-one-dimensional $\text{Rb}_2\text{Cr}_3\text{As}_3$. *Phys. Rev. B* **91**, 020506 (2015).

27. Z. T. Tang, J. K. Bao, Z. Wang, H. Bai, H. Jiang, Y. Liu, H. F. Zhai, C. M. Feng, Z. A. Xu, G. H. Cao, Superconductivity in quasi-one-dimensional $\text{Cs}_2\text{Cr}_3\text{As}_3$ with large interchain distance. *Sci. China Mater.* **58**, 16 (2015).
28. Q. G. Mu, B. B. Ruan, B. J. Pan, T. Liu, J. Yu, K. Zhao, G. F. Chen, Z. A. Ren, Ion-exchange synthesis and superconductivity at 8.6 K of $\text{Na}_2\text{Cr}_3\text{As}_3$ with quasi-one-dimensional crystal structure. *Phys. Rev. Mater.* **2**, 034803 (2018).
29. J. Yang, Z. T. Tang, G. H. Cao, Guo-qing Zheng, Ferromagnetic Spin Fluctuation and Unconventional Superconductivity in $\text{Rb}_2\text{Cr}_3\text{As}_3$ Revealed by ^{75}As NMR and NQR. *Phys. Rev. Lett.* **115**, 147002 (2015).
30. J. Luo, J. Yang, R. Zhou, Q. G. Mu, T. Liu, Z. A. Ren, C. J. Yi, Y. G. Shi, Guo-qing Zheng, Tuning the Distance to a Possible Ferromagnetic Quantum Critical Point in $\text{A}_2\text{Cr}_3\text{As}_3$. *Phys. Rev. Lett.* **123**, 047001 (2019).
31. H. Z. Zhi, T. Imai, F. L. Ning, J. K. Bao, G. H. Cao, NMR Investigation of the Quasi-One-Dimensional Superconductor $\text{K}_2\text{Cr}_3\text{As}_3$. *Phys. Rev. Lett.* **114**, 147004 (2015).
32. F. F. Balakirev, T. Kong, M. Jaime, R. D. McDonald, C. H. Mielke, A. Gurevich, P. C. Canfield, S. L. Bud'ko, Anisotropy reversal of the upper critical field at low temperatures and spin-locked superconductivity in $\text{K}_2\text{Cr}_3\text{As}_3$. *Phys. Rev. B* **91**, 220505(R) (2015).
33. G. M. Pang, M. Smidman, W. B. Jiang, J. K. Bao, Z. F. Weng, Y. F. Wang, L. Jiao, J. L. Zhang, G. H. Cao, H. Q. Yuan, Evidence for nodal superconductivity in quasi-one-dimensional $\text{K}_2\text{Cr}_3\text{As}_3$. *Phys. Rev. B* **91**, 220502(R) (2015).
34. D. T. Adroja, A. Bhattacharyya, M. Telling, Y. Feng, M. Smidman, B. Pan, J. Zhao, A. D. Hillier, F. L. Pratt, A. M. Strydom, Superconducting ground state of quasi-one-dimensional $\text{K}_2\text{Cr}_3\text{As}_3$ investigated using μSR measurements. *Phys. Rev. B* **92**, 134505 (2015).

35. A. Abragam, *The Principles of Nuclear Magnetism*, Oxford University Press, London, (1961).
36. J. Luo, C. G. Wang, Z. C. Wang, Q. Guo, J. Yang, R. Zhou, K. Matano, T. Oguchi, Z. A. Ren, G. H. Cao, Guo-qing Zheng, NMR and NQR studies on transition-metal arsenide superconductors LaRu_2As_2 , $\text{KCa}_2\text{Fe}_4\text{As}_4\text{F}_2$ and $\text{A}_2\text{Cr}_3\text{As}_3$. *Chinese Physics B*, **29**, 067402 (2020).
37. T. Moriya, *Spin Fluctuations in Itinerant Electron Magnetism*. Springer-Verlag, Berlin, 1985.
38. J. Korringa, Nuclear magnetic relaxation and resonance line shift in metals. *Physica* **16**, 601 (1950).
39. G. C. Carter, L. H. Bennet, D. J. Kahn, *Metallic shifts in NMR*. Pergamon, 1977.
40. R. Balian, N. R. Werthamer, Superconductivity with Pairs in a relative p wave. *Phys. Rev.* **131**, 1553 (1963).
41. B. Kim, S. Khmelevskiy, I. I. Mazin, D. F. Agterberg, C. Franchini, Anisotropy of magnetic interactions and symmetry of the order parameter in unconventional superconductor Sr_2RuO_4 . *npj Quantum Materials* **2**,37 (2017).
42. H. Tou, Y. Kitaoka, K. Ishida, K. Asayama, N. Kimura, Y. Onuki, E. Yamamoto, Y. Haga, K. Maezawa, Nonunitary spin-triplet superconductivity in UPt_3 : evidence from ^{195}Pt knight shift study. *Phy. Rev. Lett.* **80**, 3129 (1998).
43. H. Jiang, G. H. Cao, C. Cao, Electronic structure of quasideimensional superconductor $\text{K}_2\text{Cr}_3\text{As}_3$ from first principles calculations. *Sci. Rep.* **5**, 16054 (2015).

44. M. Nishiyama, Y. Inada, and G.-q. Zheng, Superconductivity of the ternary boride Li₂Pd₃B probed by ¹¹B NMR, *Phys. Rev. B* **71**, 220505(R) (2005).
45. J. W. F. Venderbos, V. Kozii, L. Fu, Odd-parity superconductors with two-component order parameters: Nematic and chiral, full gap, and Majorana node. *Phys. Rev. B* **94**, 180504(R) (2016).
46. W. Huang, H. Yao, Possible Three-Dimensional Nematic Odd-Parity Superconductivity in Sr₂RuO₄. *Phys. Rev. Lett.* **121**, 157002 (2018).
47. D. A. Ivanov, Non-Abelian Statistics of Half-Quantum Vortices in *p*-Wave Superconductors. *Phys. Rev. Lett.* **86**, 268 (2001).
48. G. E. Volovik, *The Universe in a Helium Droplet*, Oxford University Press, Oxford, 2002.
49. P. G. de Gennes, *Superconductivity of Metals and Alloys*. Westview Press, Oxford, 1999.
50. G. H. Cao, J. K. Bao, Z. T. Tang, Y. Liu, H. Jiang, Peculiar properties of Cr₃As₃-chain-based superconductors. *Philosophical Magazine* **97**, 591 (2017).
51. T. Kawai, C. G. Wang, Y. Kandori, Y. Honoki, K. Matano, T. Kambe, Guo-qing Zheng, Direction and symmetry transition of the vector order parameter in topological superconductors Cu_xBi₂Se₃. *Nat. Commun.* **11**, 235 (2020)
52. Y. Zhou, C. Cao, F. C. Zhang, Theory for superconductivity in alkali chromium arsenides A₂Cr₃As₃ (A = K, Rb, Cs). *Science Bulletin* **62**, 208 (2017).

Acknowledgments

We thank G.H. Cao, J.P. Hu, K. Ishida, Y. Tanaka, T. Xiang and R. Zhou for interests and useful discussion.

Funding: This work was supported by the National Key Research and Development Program of China (Nos. 2017YFA0302904, 2017YFA0302901 and 2016YFA0300502), the National Natural Science Foundation of China (Nos. 11634015, 11674377, 11774306, and 12034004), K. C. Wong Education Foundation (No. GJTD-2018-01), the Youth Innovation Promotion Association of CAS (No. 2018012), as well as JSPS (No. JP19H00657).

Author contributions: G.-q.Z designed and coordinated the project. C.J.Y and Y.G.S synthesized the single crystals. J.Y and J.L performed NMR and other measurements. Y.Z conducted group theory analysis. G.-q.Z wrote the manuscript with inputs from J.Y and Y.Z. All authors discussed the results and interpretation.

Competing interests: The authors declare no competing interests.

Data and materials availability: All data needed to evaluate the conclusions in the paper are present in the paper and/or the Supplementary Materials.

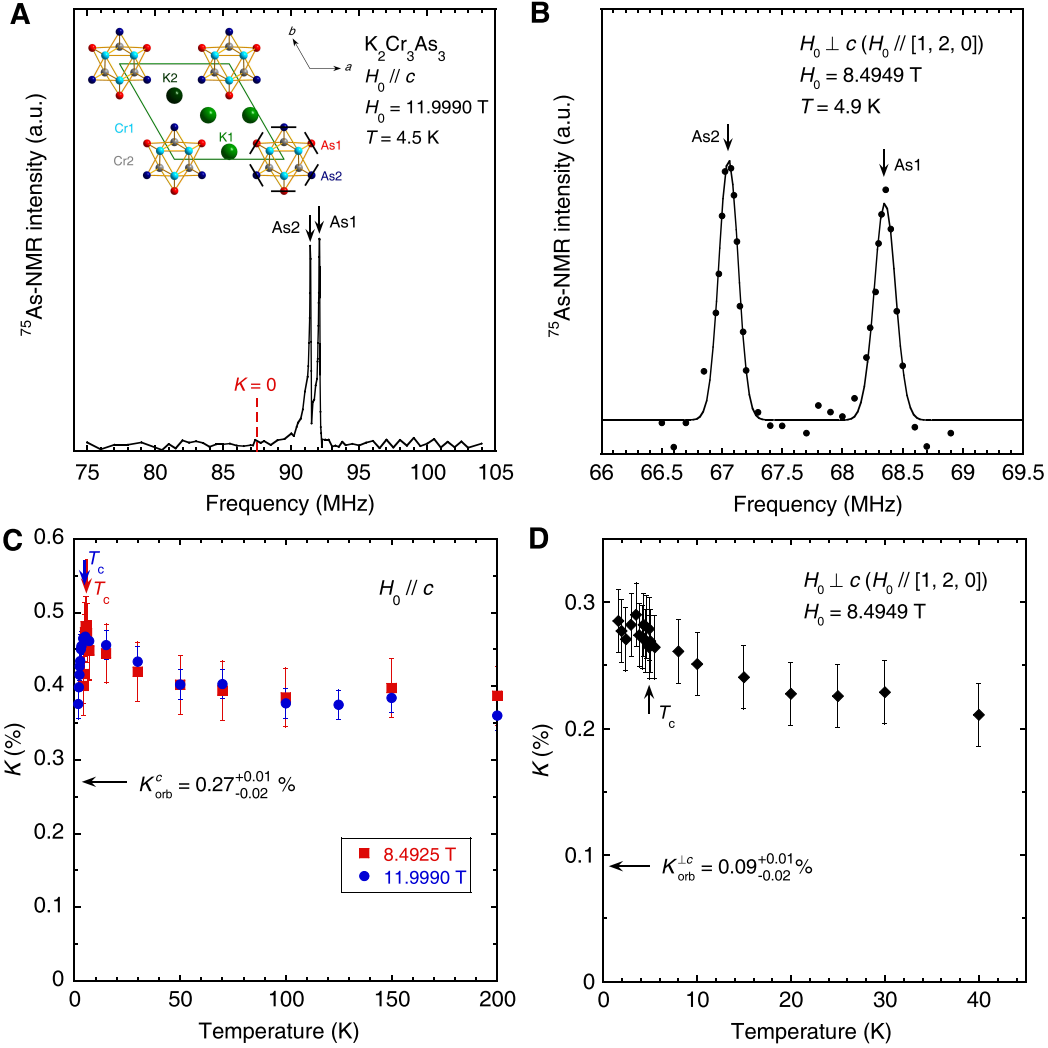


Figure 1: **NMR spectra of $K_2Cr_3As_3$ and the obtained temperature dependence of the Knight shift for the magnetic field applied along the c axis and in the ab plane.** (A, B), The ^{75}As -NMR spectra for $H_0 \parallel c$ axis, and $H_0 \parallel ab$ plane ($H_0 \parallel [1, 2, 0]$) at representative temperatures. The inset to (A) is the top view of the crystal structure of $K_2Cr_3As_3$. The green frame indicates the unit cell. There are two inequivalent As sites in the crystal lattice, i.e., As1 and As2. The principal axes of the EFG at As nuclei lie in the ab plane, which are indicated by the black bars. (C, D), The temperature dependence of the Knight shift. The vertical arrows indicate T_c under various fields, and the horizontal arrow indicate the value of Knight shift due to orbital susceptibility. The error bar for K was estimated by assuming that the spectrum-peak uncertainty equals the point (frequency) interval in measuring the NMR spectra.

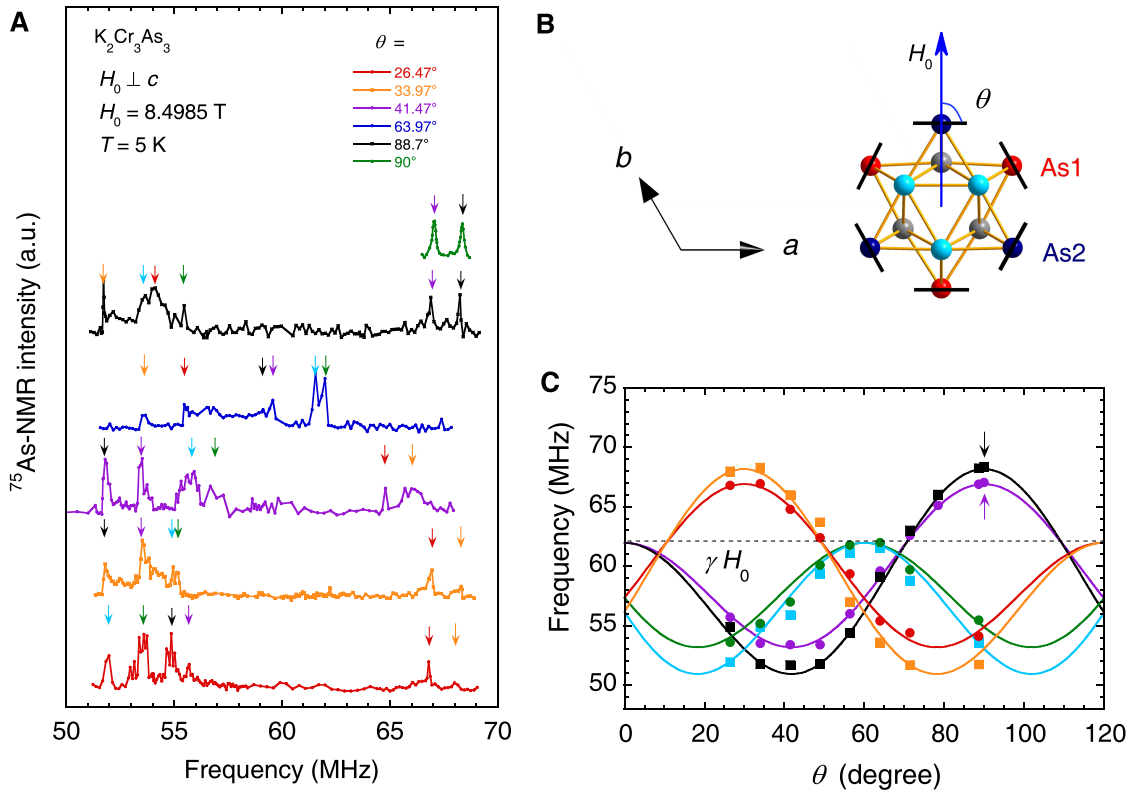


Figure 2: **Angle dependent ^{75}As NMR spectra for $H_0 \parallel ab$.** (A) Angle dependence of the complete ^{75}As NMR spectra for $H_0 \parallel ab$. The peaks are marked by the arrows with six different colors, with the same color meaning that they come from the same As position. (B) Top view of the Cr-As chains of $K_2Cr_3As_3$. The black bars indicate the directions of the EFG principal axes of the As sites. (C) Angle dependence of the ^{75}As central transition peak frequency. The curves are the theoretical calculation for the six As positions. The arrows indicate the sites and field directions at which the temperature dependence of the Knight shift was measured.

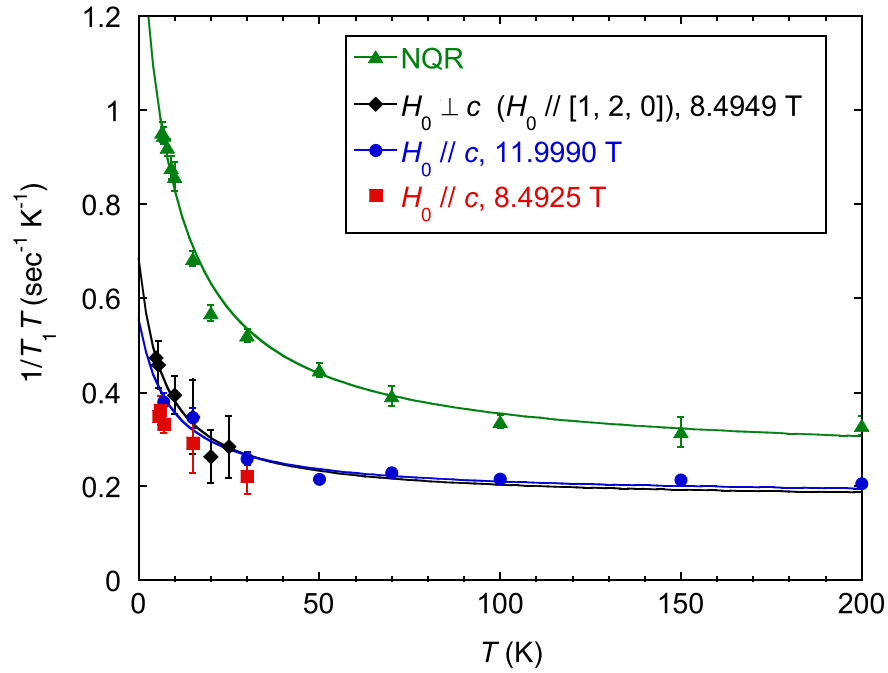


Figure 3: **Temperature dependence of $1/T_1T$ for As2 site in the normal state.** The $1/T_1T$ increases with decreasing temperature due to the development of FM spin fluctuations. The NQR data are taken from ref. (30). The solid curves are fittings to $1/T_1T = (1/T_1T)_{\text{DOS}} + b/(T + \theta)$. The error bar for $1/T_1T$ is the standard deviation in fitting the nuclear magnetization recovery curve.

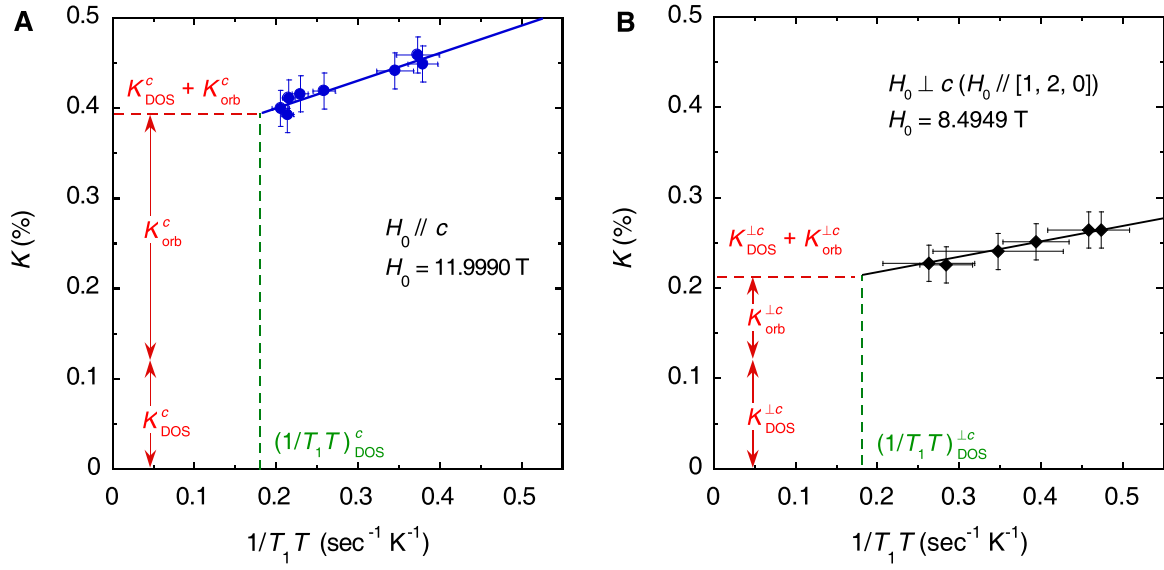


Figure 4: **Determination of the Knight shift due to orbital susceptibility (K_{orb}).** (A, B) The plot of ^{75}As Knight shift against $1/T_1T$ for $H_0 \parallel c$ axis and $H_0 \perp c$, respectively. The uncertainty for K_{orb} is $+0.01\%/ -0.02\%$.

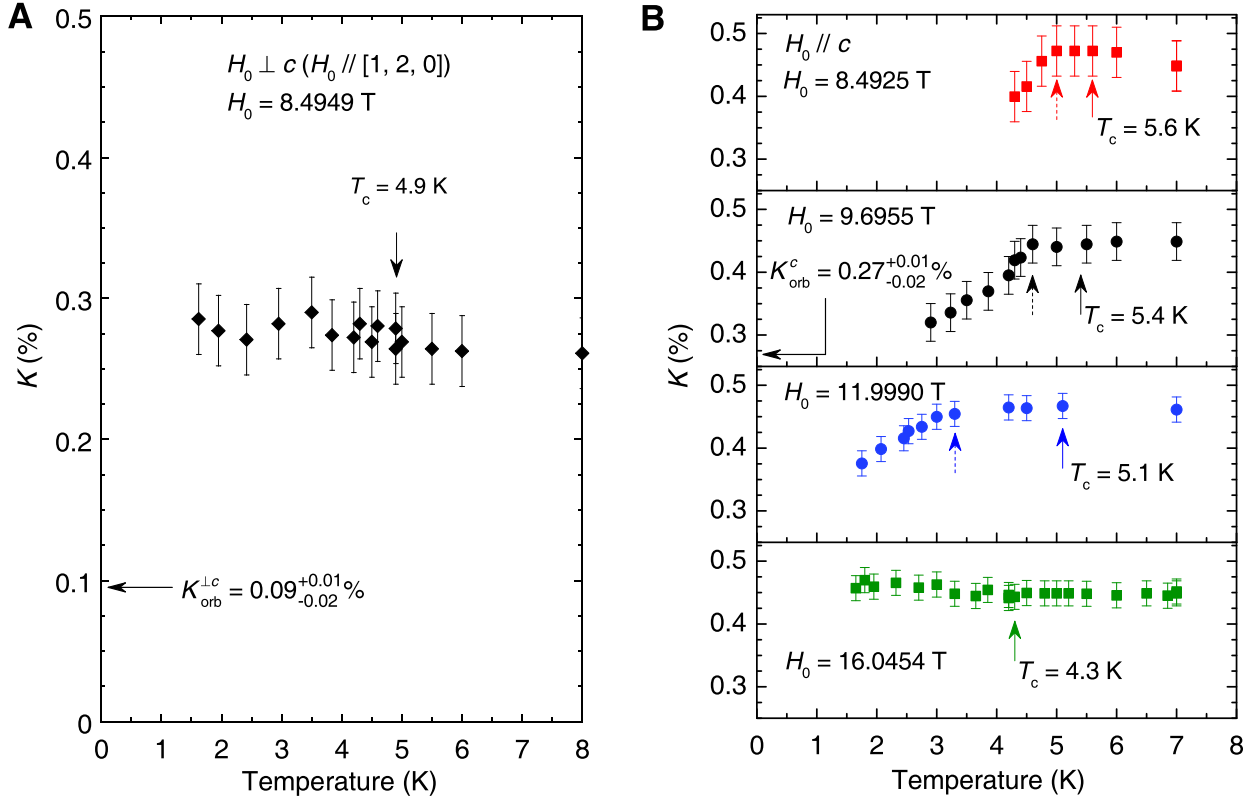


Figure 5: **Temperature dependence of the Knight shift in the superconducting state.** (A) The temperature dependence of the Knight shift with the magnetic field in the ab plane ($H_0 \parallel [1,2,0]$) (B) The Knight shift with $H_0 \parallel c$ axis. The solid arrows indicate T_c and the dotted arrows point to the temperature T^* below which the Knight shift starts to drop. The error bar for K was estimated by assuming that the spectrum-peak uncertainty equals the point (frequency) interval in measuring the NMR spectra.

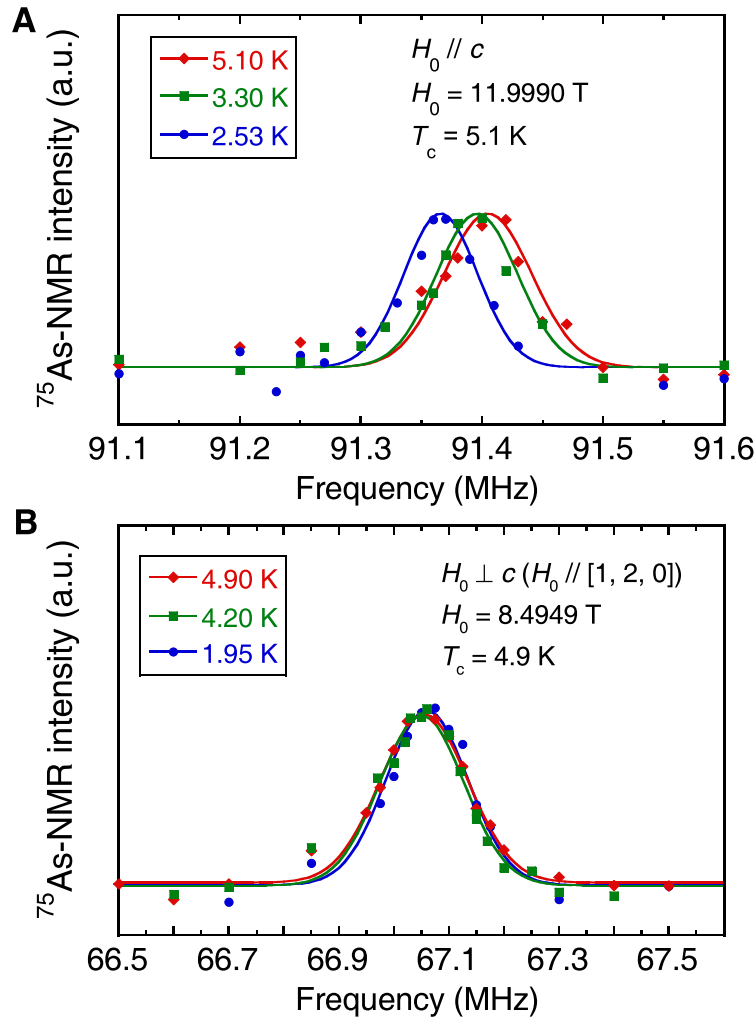


Figure 6: **Temperature dependence of the NMR spectra for $\text{K}_2\text{Cr}_3\text{As}_3$ below T_c .** (A, B) The ^{75}As NMR spectra for As2 site at representative temperatures, with the magnetic field applied parallel to the c axis and in the ab plane ($H_0 \parallel [1, 2, 0]$) direction, respectively. The solid curves are Gaussian function fittings to the spectra.

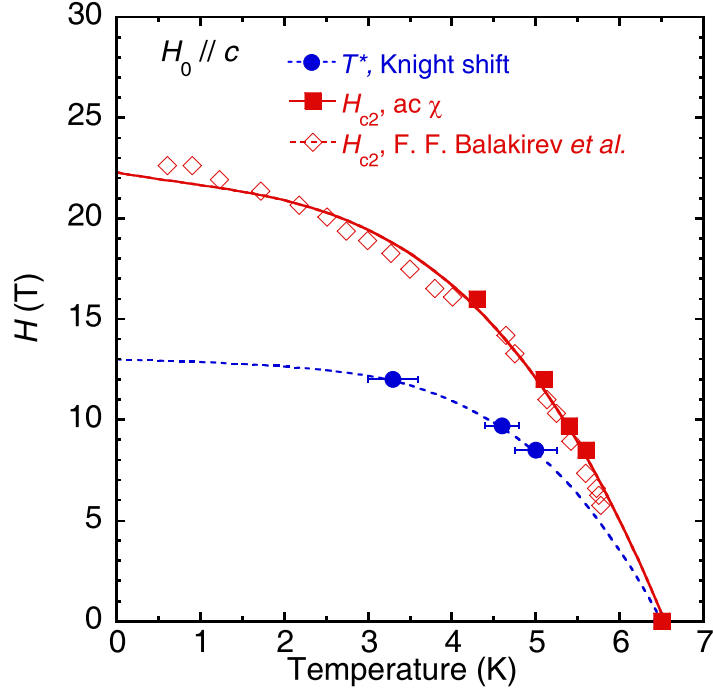


Figure 7: **The H - T phase diagram of $\text{K}_2\text{Cr}_3\text{As}_3$ with magnetic field along the c -axis.** The upper critical field data are obtained by ac susceptibility in this work (red square) and taken from ref. (32) (red diamond). T^* is the temperature at which the Knight shift starts to drop. The error bar was estimated by assuming that the uncertainty equals the point (temperature) interval around the position indicated by the broken arrow in Fig. 5B. The solid and dashed curves are guides to the eyes. Below the dashed curve, the $\vec{d}(\vec{k})$ vector is parallel to c axis. Between the solid and dashed curves, the $\vec{d}(\vec{k})$ vector is ascribed to become perpendicular to c axis (see text).

Table 1: All the possible superconducting gap functions that give rise to spin triplet and point nodes on a D_{3h} lattice.

Γ	spin-triplet $\vec{d}(k)$
E'	$(p_x \pm ip_y)\vec{z}$
A'_1	$p_x\vec{x} + p_y\vec{y}$
A''_2	$p_y\vec{x} - p_x\vec{y}$
E''	$(p_x\vec{x} - p_y\vec{y}, p_y\vec{x} + p_x\vec{y})$